

Supporting Information

High-efficiency deep-red to near-infrared emission from Pt(II) complexes by incorporating oxygen-bridged triphenylborane skeleton

Wei-Qiong Zheng,[#] Kai-Yu Lu,[#] Xiang-Qin Gan, Hu Zhang, Xiu-Qin Yan, Jun-Ting Yu, Ya-Fei Wang, Xiu-Gang Wu,^{*} and Wei-Guo Zhu^{*}

School of Materials Science and Engineering, Jiangsu Engineering Research Center of Light-Electricity-Heat Energy-Converting Materials and Applications, Jiangsu Collaborative Innovation Center of Photovoltaic Science and Engineering, Jiangsu Key Laboratories of Environment-Friendly Polymers, National Experimental Demonstration Center for Materials Science and Engineering, Changzhou University, Changzhou, 213164, P.R. China.

Email addresses: zwg@cczu.edu.cn (W. G. Zhu)

Experimental section

General Information:

^1H and ^{13}C NMR spectra were measured on a Bruker Avance III 400 and 500 MHz NMR spectrometer using CDCl_3 as the solvent and tetramethyl-silane as an internal standard at room temperature. Mass analyses were recorded by auto flex MALDI-TOF mass spectrometer. Flash EA 1112 spectrometer was used to perform the elemental analyses. Thermogravimetric analysis (TG-DTA) was performed by Bruker TG-DTA 2400SA with a heating rate of $10\text{ }^\circ\text{C min}^{-1}$ from $30\text{ }^\circ\text{C}$ to $600\text{ }^\circ\text{C}$ under nitrogen atmosphere. Cyclic voltammetry measurements were carried out on a CHI630E electrochemical workstation using a solution of 0.1 mol L^{-1} tetrabutylammonium hexafluorophosphate (Bu_4NPF_6) in dichloromethane as the supporting electrolyte at a 100 mV s^{-1} scan rate under nitrogen atmosphere. A conventional three-electrode configuration was used, consisting of a platinum spar (0.8 mm) working electrode, a platinum wire counter electrode and a KCl-saturated Ag/AgCl reference electrode.

Reagents and materials:

Experimental solvents and reagents are purchased from commercial suppliers (Bidepharm, Energy Chemistry) and used without further purification, except as otherwise mentioned. All reactions were carried out in nitrogen atmosphere using standard Schlenk line technique to avoid oxidation of the reactants in oxygen. The reaction was monitored by thin layer chromatography (TLC) until the reaction material was completely consumed. And the products were purified by column chromatography using Merck silica gel powder (100-200 mesh or 200-300 mesh).

Computational method:

The calculations were performed with Gaussian 09 program using density functional theory (DFT) and time-dependent density functional theory (TD-DFT) method with B3LYP hybrid functional. All structures were optimized using DFT (S_0 state) or TD-DFT (S_1 and T_1 states) method using 6-31G(d) basis set in gas phase. The calculations of electron density difference between ground state and excited state, and contribution of atoms to frontier molecular orbitals (FMOs) were performed by Multiwfn software (version 3.7). Natural transition orbitals (NTOs) and energy levels of singlet and triplet excited states at their optimized S_0 geometries were conducted by TD-DFT calculation at B3LYP/6-31G(d) level. The SOC matrix elements were calculated by TD-DFT at the B3LYP/def-TZVP level using ORCA software package (version 4.1).

Photophysical measurements:

Shimadzu UV-3600I Plus spectrophotometer were applied to record ultraviolet-visible (UV-Vis) absorption. The UV-Vis absorption spectra of ligands and Pt(II) complexes were measured in dichloromethane (CH_2Cl_2) solution ($1 \times 10^{-5}\text{ M}$) or in the

film prepared by spin-coating. The photoluminescence spectra were recorded on Edinburgh Instruments FLS1000 Spectrometer, and phosphorescence decay lifetimes were also measured on FLS1000 Spectrometer with time-corrected single-photon-counting (TCSPC) measurement after removing the oxygen in the solution by vacuum technique (three freeze-pump-thaw cycles). The photoluminescence quantum yields (PLQYs) of Pt(II) complexes were measured in degassed CH₂Cl₂ solutions, by an integrating sphere coupled with FLS1000 under ambient condition.

Electrochemical measurements:

CHI630e electrochemical work station was placed in a vacuum oven to measure the electrochemical property, which consist of a platinum disk as working electrode, a platinum wire as auxiliary electrode, a porous glass wick Ag/Ag⁺ as the pseudo reference electrode and ferrocene/ferrocenium as the internal standard. All measurements were performed using 0.1 M n-Bu₄NPF₆ in CH₂Cl₂ solution. Cyclic voltammetry (CV) was performed at a sweep rate of 100 mV/s. Differential pulse voltammetry (DPV) was conducted with an increment potential of 0.004 V and a pulse amplitude, width, and period of 50 mV, 0.05, and 0.5 s, respectively. The HOMO energy level (E_{HOMO}) was determined using the relation $E_{\text{HOMO}} = -(E_{\text{ox}} - 0.5 + 4.8)$ eV, where E_{ox} is the anodic peak potentials of the first oxidation peak of the DPV. The LUMO energy level (E_{LUMO}) was inferred by subtracting the optical energy gap E_{g} from the E_{HOMO} determined from the electrochemical measurements.

Device fabrication:

The optimal structure of the (BOiqn)₂Pt-doped devices is indium tin oxide (ITO)/poly(3,4-ethylenedioxythiophene)/poly(styrene sulfonate) (PEDOT:PSS) (35 nm)/tris-(4-(9*H*-carbazol-9-yl)phenyl)amine (TCTA) (20 nm)/1,3-di(9*H*-carbazol-9-yl)benzene (mCP):(BOiqn)₂Pt (14 wt%-18 wt%) (35 nm)/3,3'-[5'-[3-(pyridine-3-yl)phenyl] [1,1': 3',1''-terphenyl]-3,3''-diyl]bispyridine (TmPyPB) (50 nm)/LiF (0.5 nm)/Al (120 nm). And the optimal device structure of the (BOPy)₂Pt-doped devices is ITO/PEDOT: PSS (35 nm)/TCTA: 4,4'-di(9*H*-carbazol-9-yl)-1,1'-biphenyl (CBP) (1:1):(BOPy)₂Pt (14 wt%-18 wt%) (35 nm)/bis[2-(diphenylphosphino)phenyl] ether oxide (DPEPO) (9 nm) / TmPyPB (50 nm)/LiF (0.5 nm)/Al (120 nm). Among them, ITO served as the anode, PEDOT:PSS acted as buffer layer and hole injection layer of anode, DPEPO and TmPyPB were employed as the hole barrier layer and electron transport layer, respectively, while LiF and Al were used as electron injection layer and cathode, respectively. PEDOT:PSS were spin coated on precleaned ITO glass substrates and annealed at 160 °C for 20 min (thickness: 35 nm). Subsequently, the blend of mCP (or TCTA:CBP) and dopants in chlorobenzene solution was spin-coated directly on top of the PEDOT: PSS (thickness: 40 nm or 50 nm) as the light emitting layer. Finally, the TmPyPB films (thickness of 50 nm) were then spin-coated on the

active layer. Finally, LiF/Al electrodes were thermally evaporated through a shadow mask. The active area of the OLEDs was 4 mm². In order to avoid degradation and emission quenching caused by oxygen and moisture, all OLEDs were encapsulated in a glove box prior to the device characterization. The EL spectra and current density (*J*)-voltage (*V*)-luminance (*L*) curves were obtained using a PHOTO RESEARCH Spectra Scan PR 745 photometer and a KEITHLEY 2400 Source Meter constant current source at room temperature. The EQE values were done by calculation.

Supplementary Methods

Synthesis:

Compound 1

2, 5-dibromo-1, 3-difluorobenzene (10.00 g, 36.78 mmol), phenol (6.92 g, 73.56 mmol), potassium carbonate (20.33 g, 147.12 mmol) and *n*-methylpyrrolidone (50 mL) were mixed and reacted at 180 °C overnight. After cooling to room temperature, the mixture was mixed with water and the white solid was formed by adjusting pH = 3~4. After extraction and filtration, the solvent was removed in a vacuum at 65 °C to give **compound 1** as white solid (12.36 g, 80%). ¹H NMR (500 MHz, CDCl₃) δ 7.40 (dd, *J* = 8.6, 7.3 Hz, 4H), 7.20 (t, *J* = 7.4 Hz, 2H), 7.05 (s, 4H), 6.75 (s, 2H). ¹³C NMR (126 MHz, CDCl₃) δ 156.42, 155.80, 130.11, 124.54, 121.15, 119.19, 116.90, 105.87.

Compound 2

A solution of *n*-butyllithium in hexane (6.28 mL, 2.5 M, 15.71 mmol) was added slowly to a solution of **compound 1** (6.00 g, 14.28 mmol) in *o*-xylene (60 mL) at -30 °C under a nitrogen atmosphere. The mixture was stirred at 70 °C for 4 h and hexane was distilled off at 100 °C under a continuous flow of nitrogen. After cooled down to -30 °C, boron tribromide (4.29 g, 1.6 ml, 17.14 mmol) was added. The reaction mixture was stirred at room temperature for 2 h. *N,N*-diisopropylethylamine (3.69 g, 4.8 mL, 28.56 mmol) was added at 0 °C and then the reaction mixture was allowed to warm to room temperature for 1h. After stirring at 130 °C for 20 h, the reaction mixture was cooled to room temperature. The mixture was diluted with CH₂Cl₂ and washed with water and dried over Na₂SO₄. The solvent was removed off by a vacuum distillation and the crude product was purified by silica gel column chromatography (eluent: PE: CH₂Cl₂ = 4:1) to give **compound 2** as white solid (2.20 g, 44%). ¹H NMR (500 MHz, CDCl₃) δ 8.66 (s, 2H), 7.75 – 7.70 (m, 2H), 7.54 (d, *J* = 8.5 Hz, 2H), 7.41 (s, 4H). ¹³C NMR (101 MHz, CDCl₃) δ 160.29, 157.64, 134.56, 133.92, 128.42, 123.22, 118.54, 112.18.

BO-Bpin

Dry toluene (30 mL) was added to a 100 mL single-neck flask charged with **compound 2** (2.00 g, 5.73 mmol), pinacol diboroate (1.75 g, 6.88 mmol), potassium acetate

(2.81 g, 28.65 mmol), (dppf)PdCl₂ (0.13 g, 0.17 mmol) in nitrogen atmosphere. The mixture was stirred at 110 °C for 12 h. After cooled down to room temperature, the mixture was diluted with CH₂Cl₂ and washed with water and dried over Na₂SO₄. The solvent was removed off by a rotatory evaporation and the crude product was purified by silica gel column chromatography (PE: CH₂Cl₂ = 1:2) to give **BO-Bpin** as white solid (1.59 g, 75%). ¹H NMR (500 MHz, CDCl₃) δ 8.70 (d, *J* = 9.4 Hz, 2H), 7.76 – 7.65 (m, 4H), 7.54 (d, *J* = 7.2 Hz, 2H), 7.38 (t, *J* = 7.9 Hz, 2H), 1.41 (s, 12H). ¹³C NMR (126 MHz, CDCl₃) δ 156.87, 151.66, 151.17, 140.37, 139.47, 131.08, 127.87, 117.31, 114.97, 113.81, 55.52.

BOiqnH

BO-Bpin (760 mg, 2.05 mmol), 1-bromoisoquinoline (513 mg, 2.46 mmol), potassium carbonate (567 mg, 4.10 mmol) and Pd(PPh₃)₄ (72 mg, 0.06 mmol) were added to tetrahydrofuran/water (8/1 (*V/V*), 27 mL) solvent. The mixture was stirred and refluxed at 75 °C for 16 h. After cooled down to room temperature, the solvent was removed off by vacuum rotary evaporation, and the crude product was purified by silica gel column chromatography (PE: EA = 1:1) to give **BOiqnH** as white solid (405 mg, 50%). ¹H NMR (300 MHz, CDCl₃) δ 8.79 – 8.67 (m, 2H), 8.30 (d, *J* = 8.5 Hz, 1H), 8.01 (d, *J* = 8.2 Hz, 1H), 7.93 – 7.64 (m, 5H), 7.55 (d, *J* = 12.7 Hz, 3H), 7.43 (t, *J* = 7.4 Hz, 2H), 7.20 (t, *J* = 7.8 Hz, 1H), 7.06 (t, *J* = 7.8 Hz, 1H). ¹³C NMR (126 MHz, CDCl₃) δ 160.72, 157.29, 136.98, 134.64, 133.79, 127.69, 127.50, 127.14, 122.96, 118.62, 114.03, 110.28, 24.94.

BOPyH

BO-Bpin (400 mg, 2.05 mmol), 2-bromo-3-trifluoromethyl pyridine (293 mg, 1.30 mmol), potassium carbonate (299 mg, 2.16 mmol) and Pd(PPh₃)₄ (74 mg, 0.06 mmol) were added to tetrahydrofuran/water (8/1 (*V/V*), 27 mL) solvent. The mixture was stirred and refluxed at 75 °C for 16 h. After cooled down to room temperature, the solvent was removed off by vacuum rotary evaporation, and the crude product was purified by silica gel column chromatography (PE: EA = 1:1) to give **BOPyH** as white solid (523 mg, 61%). ¹H NMR (400 MHz, CDCl₃) δ 8.91 (d, *J* = 4.5 Hz, 1H), 8.73 (d, *J* = 6.3 Hz, 2H), 8.17 (d, *J* = 8.0 Hz, 1H), 7.73 (t, *J* = 6.9 Hz, 2H), 7.59 – 7.50 (m, 3H), 7.45 – 7.37 (m, 4H). ¹³C NMR (75 MHz, CDCl₃) δ 159.62, 155.88, 150.93, 144.30, 133.57, 132.76, 121.91, 121.36, 117.57, 108.11, 76.19, 1.03.

(BOiqn)₂Pt

Under N₂ atmosphere, **BOiqnH** (350 mg, 0.88 mmol), bis(dimethylsulphone) platinum dichloride (Pt(DMSO)₂Cl₂) (185 mg, 0.44 mmol) and sodium carbonate (280 mg, 2.64 mmol) were successively added into tetrahydrofuran (20 mL) solution. After stirring at 75 °C for 24 h, the reaction mixture was slowly turned to dark red. And then the reaction mixture was cooled to room temperature and tetrahydrofuran was removed

off under reduced pressure. The concentrated solution was extracted with CH₂Cl₂/water and dried with anhydrous sodium sulfate. After CH₂Cl₂ was distilled off and the residue was purified by silica gel column chromatography (PE: EA = 1:1) to give (BOiqn)₂Pt as red solid (160 mg, 37%). ¹H NMR (400 MHz, CDCl₃) δ 9.63 (d, *J* = 6.5 Hz, 1H), 9.37 (d, *J* = 6.5 Hz, 1H), 8.63 (ddd, *J* = 25.9, 19.1, 7.3 Hz, 4H), 8.42 (d, *J* = 8.8 Hz, 1H), 8.19 (s, 1H), 8.10 (d, *J* = 8.3 Hz, 1H), 7.98 (d, *J* = 6.5 Hz, 1H), 7.91 – 7.75 (m, 3H), 7.66 (s, 2H), 7.59 – 7.50 (m, 3H), 7.47 – 7.29 (m, 6H), 7.17 (t, *J* = 7.0 Hz, 1H), 7.01 (d, *J* = 10.5 Hz, 2H), 6.76 (s, 1H), 6.69 (d, *J* = 8.3 Hz, 1H), 5.45 (s, 1H). MALDI-TOF MS (*m/z*): 988.21353 [*M*+1]⁺; calcd for C₅₄H₃₀B₂N₂O₄Pt: 987.20394.

(BOPy)₂Pt

Under N₂ atmosphere, **BOPyH** (484 mg, 1.17 mmol), Pt(DMSO)₂Cl₂ (224 mg, 0.53 mmol) and sodium carbonate (337 mg, 3.18 mmol) were successively added into tetrahydrofuran (20 mL) solution. After stirring at 75 °C for 24 h, the reaction mixture was slowly turned to dark red. And then the reaction mixture was cooled to room temperature and tetrahydrofuran was removed off under reduced pressure. The concentrated solution was extracted with CH₂Cl₂/water and dried with anhydrous sodium sulfate. After CH₂Cl₂ was distilled off and the residue was purified by silica gel column chromatography (PE: CH₂Cl₂ = 1:2) to give (BOPy)₂Pt as red solid (220 mg, 41%). ¹H NMR (400 MHz, CDCl₃) δ 10.05 (d, *J* = 5.8 Hz, 1H), 9.70 (d, *J* = 5.8 Hz, 1H), 8.74 (t, *J* = 6.5 Hz, 2H), 8.56 (dd, *J* = 22.9, 7.5 Hz, 2H), 8.45 (d, *J* = 8.1 Hz, 1H), 8.05 (d, *J* = 8.1 Hz, 1H), 7.91 (s, 1H), 7.84 – 7.77 (m, 1H), 7.72 – 7.63 (m, 2H), 7.53 – 7.29 (m, 7H), 7.22 (d, *J* = 7.1 Hz, 1H), 7.16 (t, *J* = 7.0 Hz, 1H), 6.56 – 6.46 (m, 2H), 5.89 (d, *J* = 8.4 Hz, 1H). MALDI-TOF MS(*m/z*): 1024.15529 [*M*+1]⁺; calcd for C₄₈H₂₄B₂F₆N₂O₄Pt: 1023.14741.

(piq)₂Pt

Under N₂ atmosphere, 1-phenylisoquinoline (306 mg, 1.49 mmol), Pt(DMSO)₂Cl₂ (300 mg, 0.71 mmol) and sodium carbonate (452 mg, 4.62 mmol) were successively added into tetrahydrofuran (30 mL) solution. After stirring at 75 °C for 24 h, the reaction mixture was slowly turned to dark. And then the reaction mixture was cooled to room temperature and tetrahydrofuran was removed off under reduced pressure. The concentrated solution was extracted with CH₂Cl₂/water and dried with anhydrous sodium sulfate. After CH₂Cl₂ was distilled off and the residue was purified by silica gel column chromatography (PE: EA = 1:1) to give (piq)₂Pt as brown solid (70 mg, 16%). ¹H NMR (400 MHz, CDCl₃) δ 8.92 (s, 1H), 8.62 (s, 2H), 7.96 (s, 2H), 7.82 (s, 6H), 7.75 (s, 4H), 7.64 – 7.58 (m, 3H), 7.55 (s, 2H). ¹³C NMR (100 MHz, CDCl₃) δ 143.50, 131.94, 130.58, 129.28, 128.29, 128.17, 128.00, 126.05, 125.93, 121.97, 44.09, 41.96, -1.03.

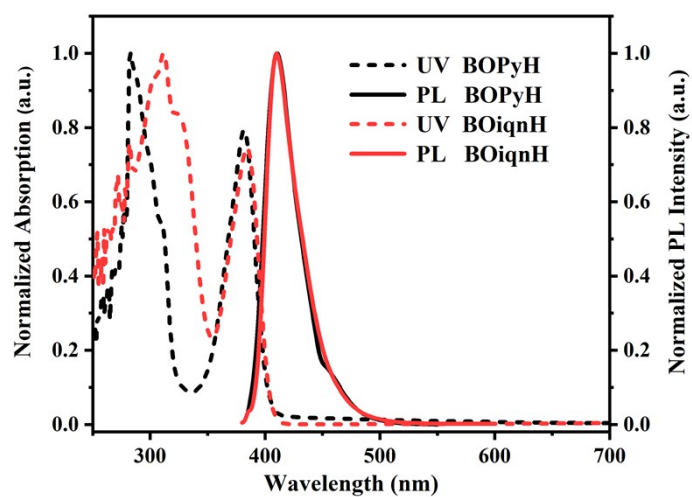


Figure S1 UV-Vis absorption and PL spectra of ligand BOPyH and BOiqnH in CH_2Cl_2 solution (1×10^{-5} M) at 298 K.

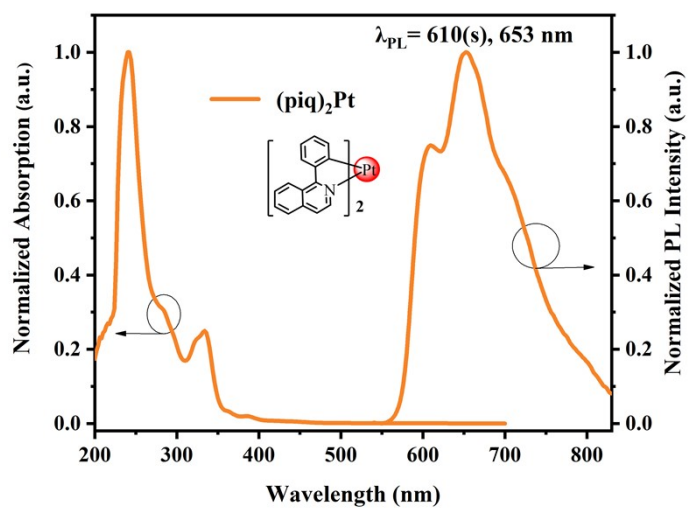


Figure S2 UV-Vis absorption and PL spectra of complex $(\text{piq})_2\text{Pt}$ in degassed CH_2Cl_2 solution (1×10^{-5} M) at 298 K.

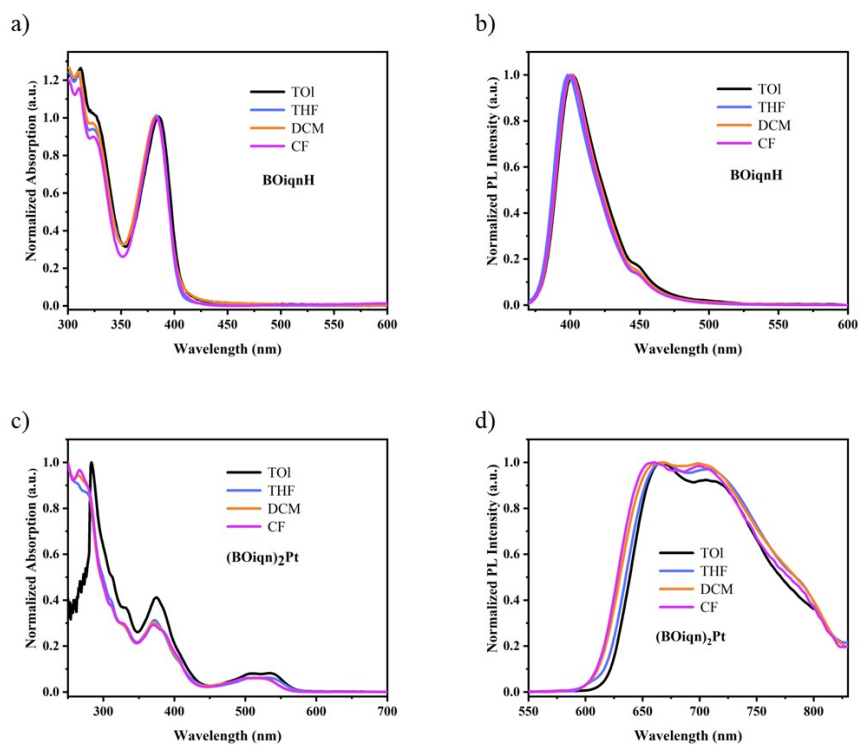


Figure S3 UV-Vis and PL spectra of BOiqnH ($\lambda_{\text{ex}} = 380$ nm) (a,b) and (BOiqn)₂Pt ($\lambda_{\text{ex}} = 520$ nm) (c,d) at RT in different solvents under same measurement conditions.

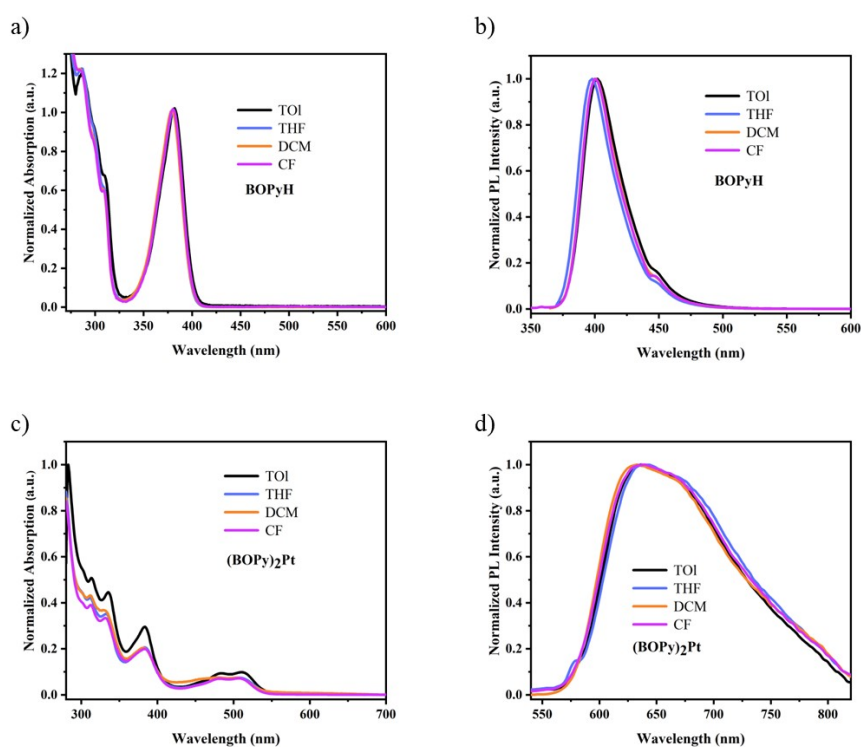


Figure S4 UV-Vis and PL spectra of BOPyH ($\lambda_{\text{ex}} = 380$ nm) (a,b) and (BOPy)₂Pt ($\lambda_{\text{ex}} = 510$ nm) (c,d) at RT in different solvents under same measurement conditions.

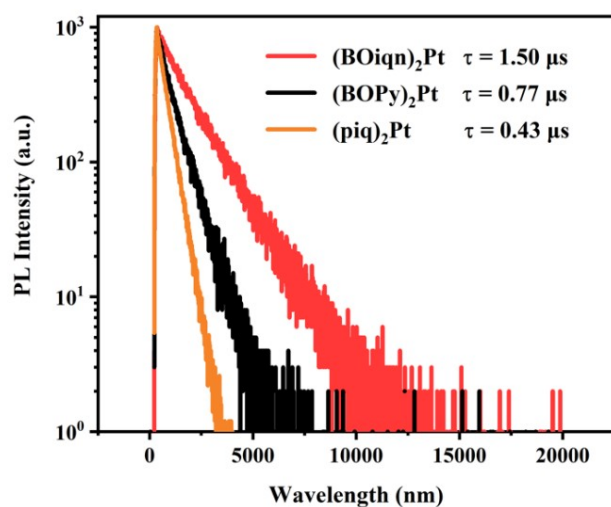


Figure S5 Transient PL decay spectra of (BOiqn)₂Pt, (BOPy)₂Pt and (piq)₂Pt in degassed CH₂Cl₂ solution at 298 K (concentration: 1 × 10⁻⁵ M)

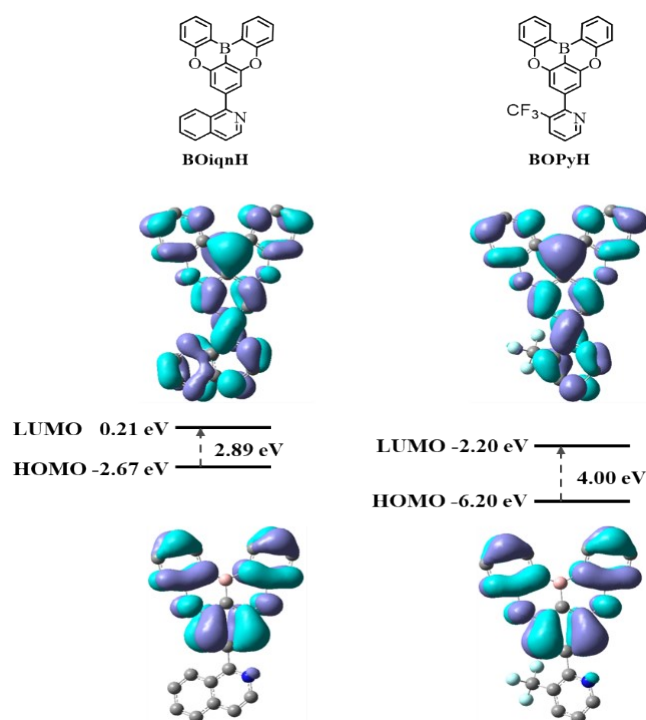


Figure S6 The frontier molecular orbital distributions, energy levels and gaps of BOiqnH and BOPyH obtained by DFT calculation (The H atom is omitted for clarity)

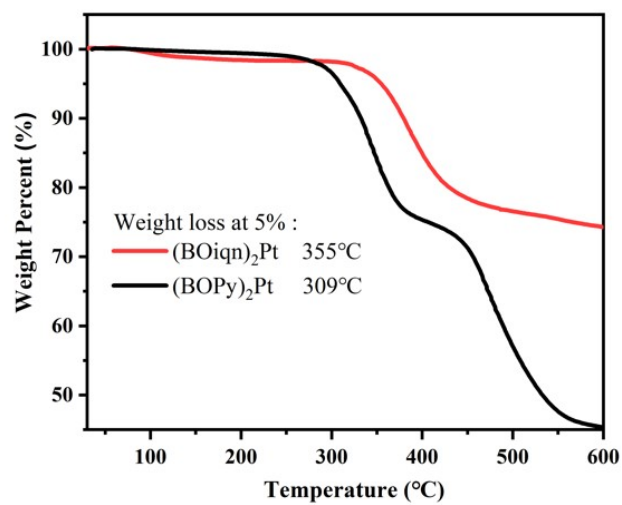


Figure S7 TGA curves of (BOiqn)₂Pt and (BOPy)₂Pt under N₂ with a rate of 20°C/min

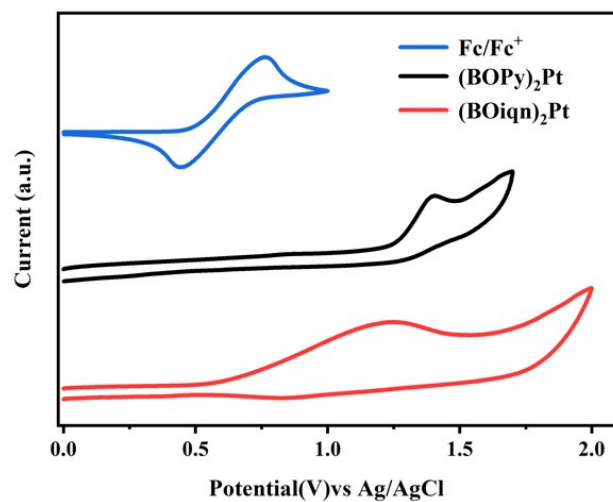


Figure S8 CV curves of (BOiqn)₂Pt and (BOPy)₂Pt in degassed CH₂Cl₂ solution.

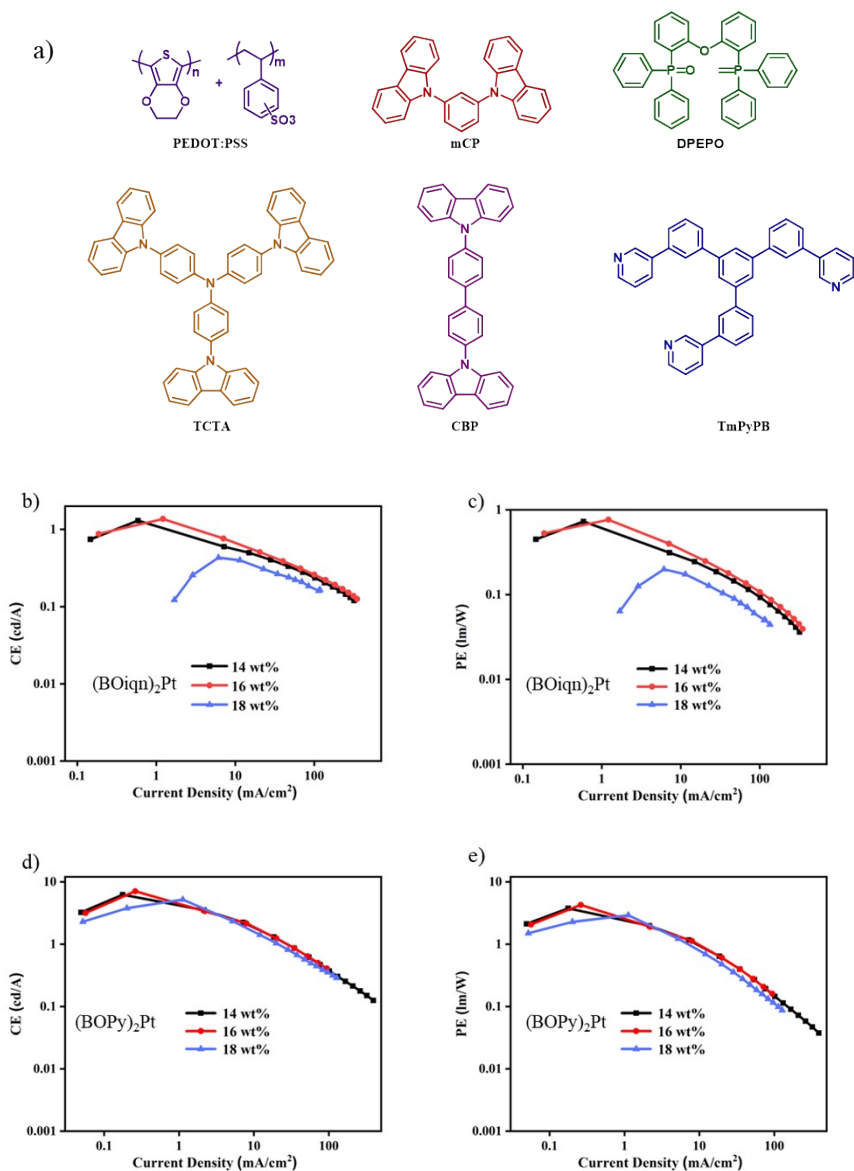


Figure S9 (a) Chemical structures of the relevant materials, current efficiency–luminance characteristics and power efficiency–luminance characteristics of doped devices based on (BOiqn)₂Pt (b)(c) and (BOPy)₂Pt (d)(e).

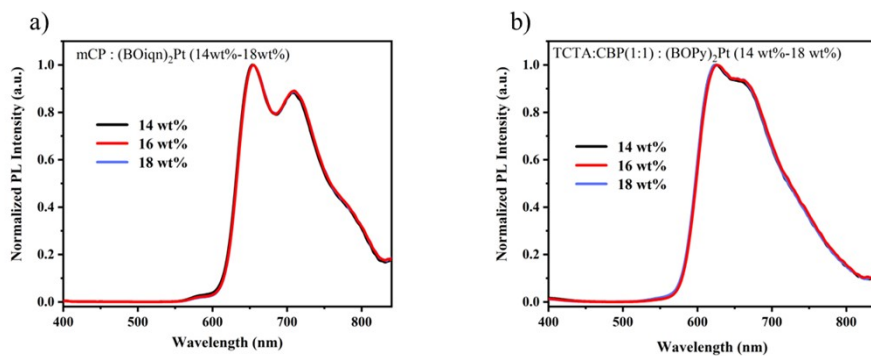


Figure S10. PL spectra of the (BOiqn)₂Pt (a) and (BOPy)₂Pt (b) doped films at different dopant concentrations.

Table S1 Contribution of atoms to HOMOs and LUMOs for (BOiqn)₂Pt by orbital composition analysis using Hirshfeld method performed on Multiwfn software package (version 3.7).

Atom	Contribution (%)		Atom	Contribution (%)		Atom	Contribution (%)	
	HOMO	LUMO		HOMO	LUMO		HOMO	LUMO
1(Pt)	20.35%	2.72%	32(H)	0.00%	0.00%	63(H)	0.00%	0.00%
2(C)	0.08%	0.50%	33(H)	0.00%	0.00%	64(H)	0.04%	0.04%
3(C)	1.29%	0.09%	34(H)	0.00%	0.00%	65(H)	0.00%	0.00%
4(C)	0.06%	0.49%	35(H)	0.00%	0.00%	66(H)	0.00%	0.00%
5(C)	0.87%	0.23%	36(C)	0.08%	0.50%	67(H)	0.00%	0.00%
6(C)	0.40%	0.20%	37(C)	1.29%	0.09%	68(H)	0.00%	0.00%
7(C)	1.06%	0.02%	38(C)	0.06%	0.49%	69(H)	0.01%	0.05%
8(O)	3.43%	0.36%	39(C)	0.87%	0.23%	70(H)	0.01%	0.05%
9(C)	4.53%	0.79%	40(C)	0.40%	0.20%	71(H)	0.00%	0.00%
10(C)	4.85%	1.88%	41(C)	1.06%	0.02%	72(C)	0.04%	3.93%
11(C)	2.24%	1.49%	42(O)	3.43%	0.36%	73(C)	0.15%	0.20%
12(C)	7.73%	2.23%	43(C)	4.53%	0.79%	74(C)	0.10%	1.75%
13(C)	4.53%	0.41%	44(C)	4.85%	1.88%	75(C)	0.03%	2.47%
14(C)	0.14%	1.52%	45(C)	2.24%	1.49%	76(C)	0.06%	3.68%
15(B)	0.05%	2.23%	46(C)	7.73%	2.23%	77(C)	0.07%	0.95%
16(C)	0.03%	0.39%	47(C)	4.53%	0.41%	78(H)	0.03%	0.02%
17(C)	1.24%	0.11%	48(C)	0.14%	1.52%	79(H)	0.00%	0.00%
18(C)	0.12%	0.43%	49(B)	0.05%	2.23%	80(H)	0.00%	0.00%
19(C)	1.17%	0.02%	50(C)	0.03%	0.39%	81(H)	0.00%	0.01%
20(C)	0.30%	0.20%	51(C)	1.24%	0.11%	82(C)	0.25%	5.17%
21(C)	0.91%	0.23%	52(C)	0.12%	0.42%	83(C)	0.15%	0.20%
22(O)	3.31%	0.29%	53(C)	1.17%	0.02%	84(C)	0.04%	3.93%
23(C)	0.13%	10.70%	54(C)	0.30%	0.20%	85(C)	0.07%	0.95%
24(C)	0.25%	5.17%	55(C)	0.91%	0.23%	86(C)	0.06%	3.68%
25(C)	0.16%	0.18%	56(O)	3.31%	0.29%	87(C)	0.03%	2.47%
26(N)	0.42%	5.38%	57(C)	0.13%	10.70%	88(C)	0.10%	1.75%
27(H)	0.00%	0.00%	58(C)	0.16%	0.18%	89(H)	0.03%	0.02%
28(H)	0.00%	0.00%	59(N)	0.42%	5.38%	90(H)	0.00%	0.01%
29(H)	0.00%	0.00%	60(H)	0.00%	0.00%	91(H)	0.00%	0.00%
30(H)	0.00%	0.00%	61(H)	0.00%	0.00%	92(H)	0.00%	0.00%
31(H)	0.04%	0.04%	62(H)	0.00%	0.00%	93(H)	0.00%	0.00%

Table S2 Contribution of atoms to HOMOs and LUMOs for (BOPy)₂Pt by orbital composition analysis using Hirshfeld method performed on Multiwfn software package (version 3.7).

Atom	Contribution (%)		Atom	Contribution (%)		Atom	Contribution (%)	
	HOMO	LUMO		HOMO	LUMO		HOMO	LUMO
1(Pt)	17.52%	2.97%	30(H)	0.00%	0.00%	59(C)	0.15%	10.28%
2(C)	0.08%	0.72%	31(H)	0.00%	0.00%	60(C)	0.16%	0.54%
3(C)	1.37%	0.11%	32(H)	0.00%	0.01%	61(C)	0.19%	5.36%
4(C)	0.08%	0.73%	33(H)	0.03%	0.00%	62(C)	0.13%	1.12%
5(C)	0.90%	0.33%	34(H)	0.00%	0.00%	63(N)	0.34%	6.29%
6(C)	0.45%	0.25%	35(H)	0.00%	0.00%	64(H)	0.00%	0.00%
7(C)	1.22%	0.03%	36(H)	0.00%	0.00%	65(H)	0.00%	0.00%
8(O)	3.82%	0.51%	37(H)	0.00%	0.00%	66(H)	0.00%	0.00%
9(C)	4.51%	1.15%	38(C)	0.08%	0.72%	67(H)	0.00%	0.01%
10(C)	5.53%	2.16%	39(C)	1.37%	0.11%	68(H)	0.03%	0.00%
11(C)	1.76%	2.10%	40(C)	0.08%	0.72%	69(H)	0.00%	0.00%
12(C)	7.75%	2.59%	41(C)	0.91%	0.33%	70(H)	0.00%	0.00%
13(C)	4.61%	0.48%	42(C)	0.45%	0.25%	71(H)	0.00%	0.00%
14(C)	0.13%	1.72%	43(C)	1.22%	0.03%	72(H)	0.00%	0.00%
15(B)	0.05%	2.99%	44(O)	3.82%	0.51%	73(H)	0.01%	0.06%
16(C)	0.04%	0.52%	45(C)	4.51%	1.14%	74(H)	0.01%	0.06%
17(C)	1.48%	0.16%	46(C)	5.53%	2.16%	75(C)	0.10%	6.55%
18(C)	0.16%	0.57%	47(C)	1.76%	2.10%	76(H)	0.00%	0.01%
19(C)	1.23%	0.02%	48(C)	7.75%	2.59%	77(H)	0.01%	0.00%
20(C)	0.41%	0.26%	49(C)	4.61%	0.48%	78(H)	0.00%	0.01%
21(C)	1.06%	0.31%	50(C)	0.13%	1.72%	79(H)	0.01%	0.00%
22(O)	3.45%	0.36%	51(B)	0.05%	2.98%	80(C)	0.02%	0.15%
23(C)	0.15%	10.29%	52(C)	0.04%	0.52%	81(C)	0.02%	0.15%
24(C)	0.16%	0.55%	53(C)	1.48%	0.16%	82(F)	0.01%	0.02%
25(C)	0.10%	6.55%	54(C)	0.16%	0.57%	83(F)	0.01%	0.05%
26(C)	0.19%	5.36%	55(C)	1.23%	0.02%	84(F)	0.01%	0.01%
27(C)	0.13%	1.12%	56(C)	0.41%	0.26%	85(F)	0.01%	0.02%
28(N)	0.34%	6.29%	57(C)	1.06%	0.31%	86(F)	0.01%	0.01%
29(H)	0.00%	0.00%	58(O)	3.45%	0.35%	87(F)	0.01%	0.05%

Table S3. TD-DFT results for complex based on their optimized S_0 geometries

complex		(BOiqn) ₂ Pt/%				(BOPy) ₂ Pt/%				(piq) ₂ Pt/%			
MOs ^a		L+1	L	H	H-1	L+1	L	H	H-1	L+1	L	H	H-1
contribution	Pt	3.27	2.71	20.35	8.83	1.93	2.96	17.51	5.38	2.91	4.91	34.61	21.43
percentages of													
molecular													
moieties to	Ligand	96.73	97.29	79.65	91.17	98.07	97.04	82.49	94.62	97.09	95.09	65.39	78.57
MOs/%													
main configuration of $S_0 \rightarrow S_1$		H \rightarrow L (69.6 %)				H \rightarrow L (76.1 %)				H \rightarrow L (70.1 %)			
excitation / $E_{cal}/\lambda_{cal}/$ character ^b		2.00 eV				2.14 eV				2.14 eV			
		621 nm				578 nm				579 nm			
		$\pi(\text{BOiqn})/d_{\pi}(\text{Pt}) \rightarrow \pi^*(\text{BOiqn})$				$\pi(\text{BOPy})/d_{\pi}(\text{Pt}) \rightarrow \pi^*(\text{BOPy})$				$\pi(\text{piq})/d_{\pi}(\text{Pt}) \rightarrow \pi^*(\text{piq})$			
main configuration of $S_0 \rightarrow T_1$		H-1 \rightarrow L+1 (14.6 %)				H-1 \rightarrow L+1 (17.5 %)				H-1 \rightarrow L (19.3 %)			
excitation / $E_{cal}/\lambda_{cal}/$ character ^b		H \rightarrow L (67.9%)				H \rightarrow L (67.4 %)				H \rightarrow L (63.9 %)			
		1.77 eV				1.87 eV				1.90 eV			
		699 nm				661 nm				650 nm			
		$\pi(\text{BOiqn})/d_{\pi}(\text{Pt}) \rightarrow \pi^*(\text{BOiqn})$				$\pi(\text{BOPy})/d_{\pi}(\text{Pt}) \rightarrow \pi^*(\text{BOPy})$				$\pi(\text{piq})/d_{\pi}(\text{Pt}) \rightarrow \pi^*(\text{piq})$			

^a H and L denote molecular orbitals (MO) HOMO and LUMO, respectively. ^b E_{cal} and λ_{cal} represent calculated excitation energies and corresponding wavelengths, data in parentheses are the contributions of corresponding excitations.

Table S4. Excited state properties of (BOiqn)₂Pt obtained from TD-DFT calculations carried out at the ground tripletstate(S₀) geometry.

Complex	State (<i>E</i> , <i>λ</i>)	Dominant excitations	Oscillator strength	Character
(BOiqn) ₂ Pt	S ₁ (2.00 eV, 621 nm)	HOMO→LUMO (69.6)	0.0868	ILCT/MLCT
	S ₂ (2.33 eV, 531 nm)	HOMO-1→LUMO (12.5) HOMO→LUMO+1 (68.5)	0.0093	ILCT/MLCT
	S ₃ (2.42 eV, 510 nm)	HOMO-4→LUMO (11.7) HOMO-1→LUMO (68.1) HOMO→LUMO+1 (12.5)	0.0003	ILCT/MLCT
	S ₄ (2.76eV, 447 nm)	HOMO-3→LUMO+1 (11.9) HOMO-1→LUMO+1 (68.1)	0.0028	ILCT/MLCT
	S ₅ (2.86 eV, 432 nm)	HOMO-8→LUMO (11.8) HOMO-3→LUMO (68.1)	0.2072	ILCT/MLCT
	T ₁ (1.77 eV, 699 nm)	HOMO-1→LUMO+1 (14.6) HOMO→LUMO (67.9)	triplet	ILCT/MLCT
	T ₂ (1.96 eV, 631 nm)	HOMO-1→LUMO (41.7) HOMO→LUMO+1 (53.1)	triplet	ILCT/MLCT
	T ₃ (2.23 eV, 554 nm)	HOMO-5→LUMO+1 (16.1) HOMO-4→LUMO (13.4) HOMO-3→LUMO+1 (23.1) HOMO-2→LUMO (54.4) HOMO-1→LUMO+1 (14.4)	triplet	ILCT/MLCT/LLCT
	T ₄ (2.27 eV, 545 nm)	HOMO-5→LUMO (12.9) HOMO-3→LUMO (31.3) HOMO-2→LUMO+1 (26.2) HOMO-1→LUMO (31.9) HOMO→LUMO+1 (38.5)	triplet	ILCT/MLCT/LLCT
	T ₅ (2.53 eV, 488 nm)	HOMO-4→LUMO (10.5) HOMO-2→LUMO (2.3) HOMO-1→LUMO+1 (76.1) HOMO-1→LUMO+3 (5.1) HOMO→LUMO (31.9) HOMO→LUMO+2 (38.5)	triplet	ILCT/MLCT/LLCT

Table S5. Excited state properties of (BOPy)₂Pt obtained from TD-DFT calculations carried out at the ground state(S₀) geometry.

Complex	State (<i>E</i> , <i>λ</i>)	Dominant excitations	Oscillator strength	Character
(BOPy)₂Pt	S ₁ (2.14 eV, 578 nm)	HOMO→LUMO (76.1)	0.0916	ILCT/MLCT
	S ₂ (2.48 eV, 498 nm)	HOMO→LUMO+1 (69.0)	0.0066	ILCT/MLCT
	S ₃ (2.57 eV, 481 nm)	HOMO-1→LUMO (96.6)	0.0005	ILCT/MLCT
	S ₄ (2.69 eV, 460 nm)	HOMO→LUMO+2 (69.6)	0.0156	ILCT/MLCT
	S ₅ (2.86 eV, 433 nm)	HOMO→LUMO+3 (69.7)	0.0000	ILCT/MLCT
	T ₁ (1.87 eV, 661 nm)	HOMO-1→LUMO+1(17.5) HOMO→LUMO (67.4)	triplet	ILCT/MLCT
	T ₂ (2.07 eV, 598nm)	HOMO-1→LUMO (39.9) HOMO→LUMO+1 (56.1)	triplet	ILCT/MLCT
	T ₃ (2.49 eV, 496 nm)	HOMO-3→LUMO (11.2) HOMO-1→LUMO (54.8) HOMO→LUMO+1 (39.5)	triplet	ILCT/MLCT/LLCT
	T ₄ (2.50 eV, 494 nm)	HOMO-2→LUMO (14.4) HOMO-1→LUMO+1 (38.7) HOMO→LUMO (13.1) HOMO→LUMO+2 (53.4)	triplet	ILCT/MLCT/LLCT
	T ₅ (2.71 eV, 456 nm)	HOMO-7→LUMO+1 (18.3) HOMO-6→LUMO (18.3) HOMO-4→LUMO (38.5) HOMO-3→LUMO+1 (20.7) HOMO-2→LUMO+1 (36.3)	triplet	ILCT/MLCT/LLCT

Table S6. Excited state properties of (piq)₂Pt obtained from TD-DFT calculations carried out at the ground state(S₀) geometry.

Complex	State (<i>E</i> , <i>λ</i>)	Dominant excitations	Oscillator strength	Character
(piq) ₂ Pt	S ₁ (2.14 eV, 579 nm)	HOMO→LUMO (70.1)	0.0560	ILCT/MLCT
	S ₂ (2.51 eV, 493 nm)	HOMO→LUMO+1 (72.6)	0.0003	ILCT/MLCT
	S ₃ (2.76 eV, 449 nm)	HOMO-5→LUMO (10.1) HOMO-4→LUMO (11.0) HOMO-1→LUMO (68.3)	0.0415	ILCT/MLCT
	S ₄ (2.77 eV, 446 nm)	HOMO-3→LUMO (31.6) HOMO-2→LUMO (62.3)	0.0007	ILCT/MLCT
	S ₅ (3.10 eV, 398 nm)	HOMO-4→LUMO (34.3) HOMO-3→LUMO+1 (54.1) HOMO-2→LUMO+1 (8.6)	0.0110	ILCT/MLCT
	T ₁ (1.90 eV, 650 nm)	HOMO-3→LUMO+1(10.9) HOMO-2→LUMO+1 (15.0) HOMO-1→LUMO (19.3) HOMO→LUMO (63.9)	triplet	ILCT/MLCT
	T ₂ (2.11 eV, 585 nm)	HOMO-3→LUMO (24.2) HOMO-2→LUMO (38.8) HOMO-1→LUMO+1 (34.6) HOMO→LUMO+1 (36.4)	triplet	ILCT/MLCT
	T ₃ (2.16 eV, 573 nm)	HOMO-3→LUMO+1 (17.6) HOMO-2→LUMO+1 (20.8) HOMO-1→LUMO (56.4) HOMO→LUMO (26.3)	triplet	ILCT/MLCT/LLCT
	T ₄ (2.38 eV, 519 nm)	HOMO-3→LUMO (12.7) HOMO-2→LUMO (16.4) HOMO-1→LUMO+1 (28.7) HOMO→LUMO+1 (58.5)	triplet	ILCT/MLCT/LLCT
	T ₅ (2.68 eV, 461 nm)	HOMO-3→LUMO (48.0) HOMO-2→LUMO (47.4) HOMO-1→LUMO+1 (12.0)	triplet	ILCT/MLCT/LLCT

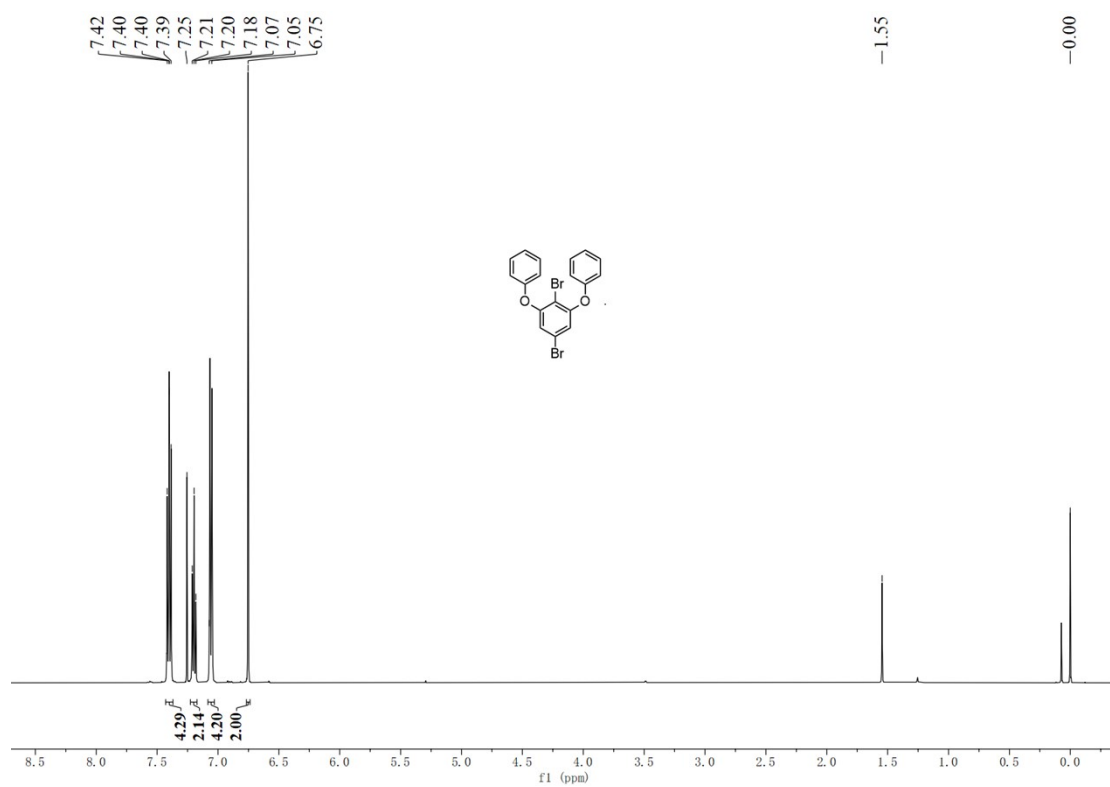


Figure S11 $^1\text{H-NMR}$ spectrum of compound 1

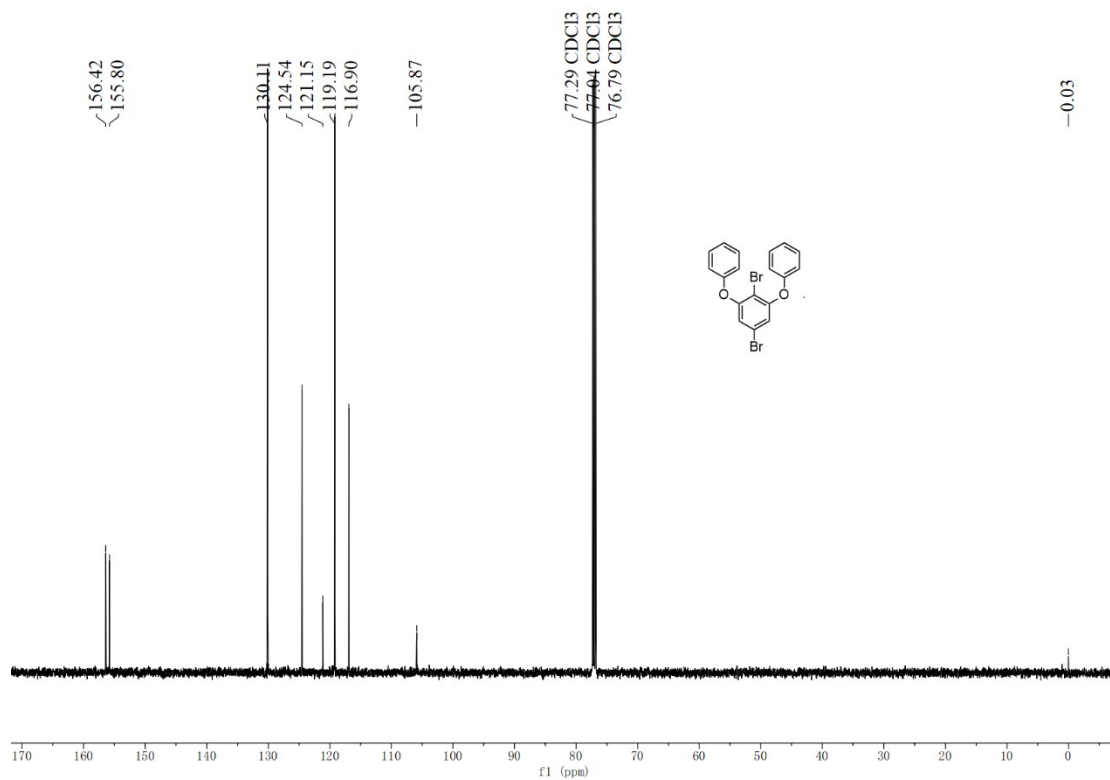


Figure S12 $^{13}\text{C-NMR}$ spectrum of compound 1

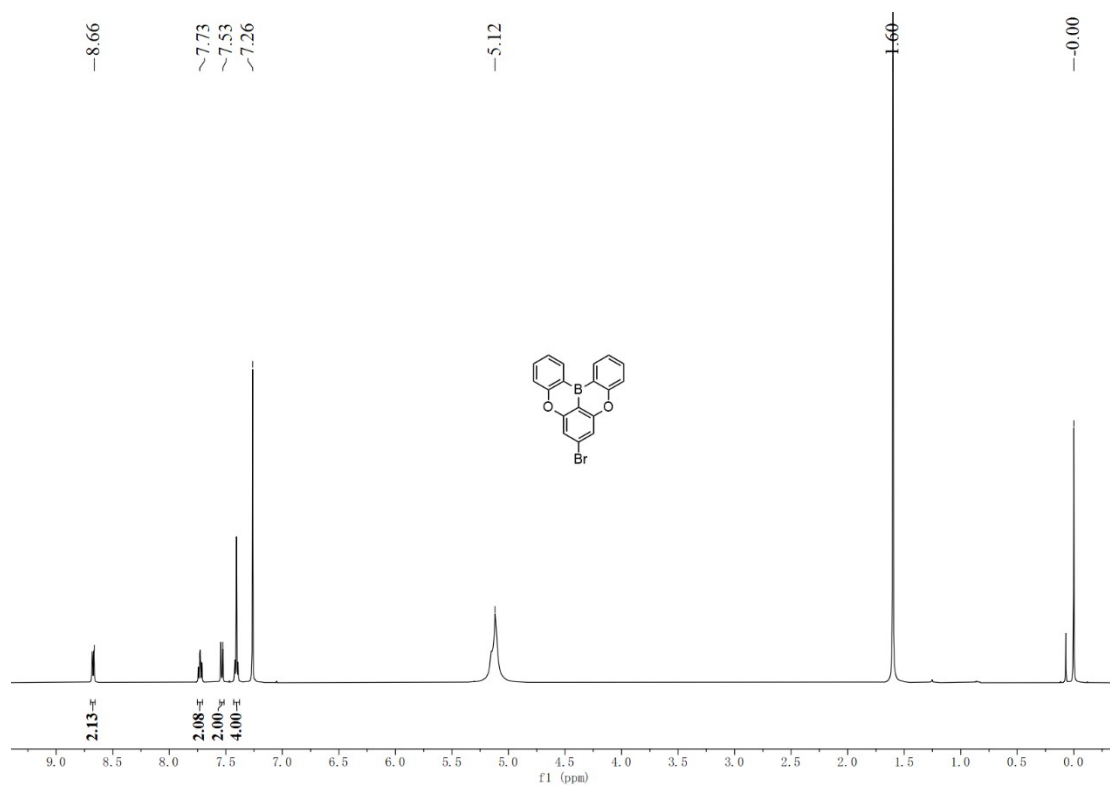


Figure S13 ¹H-NMR spectrum of compound 2

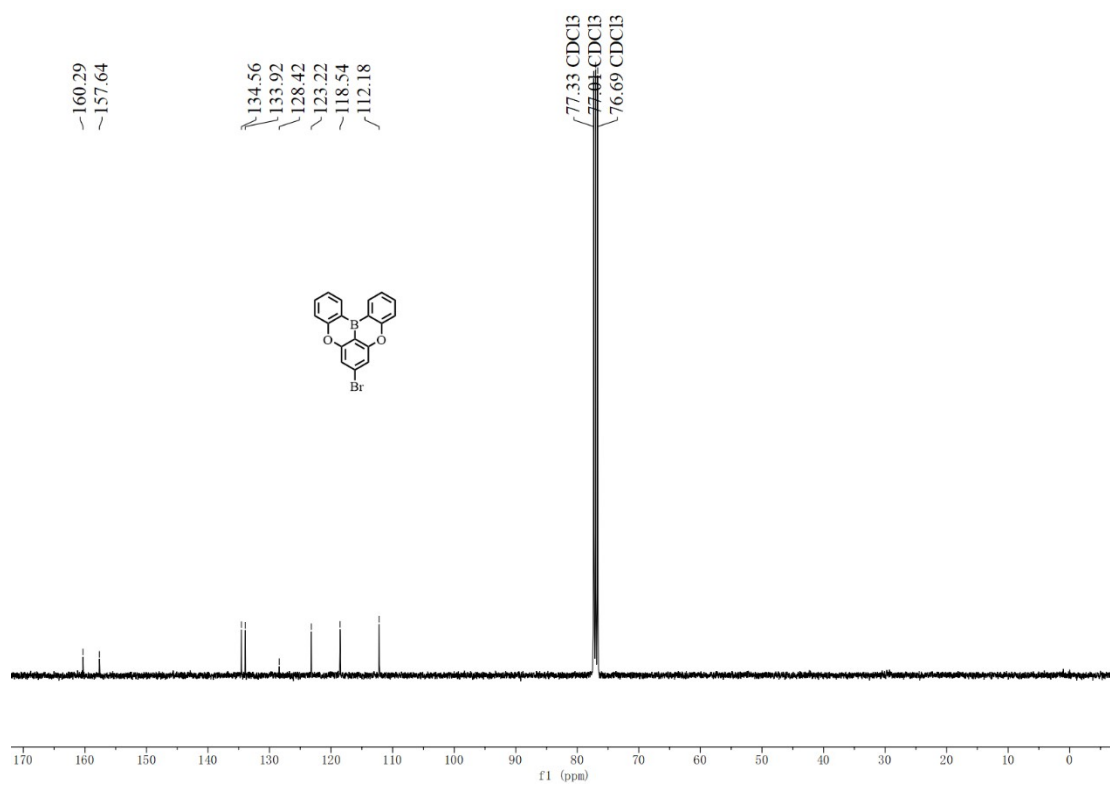


Figure S14 ¹³C-NMR spectrum of compound 2

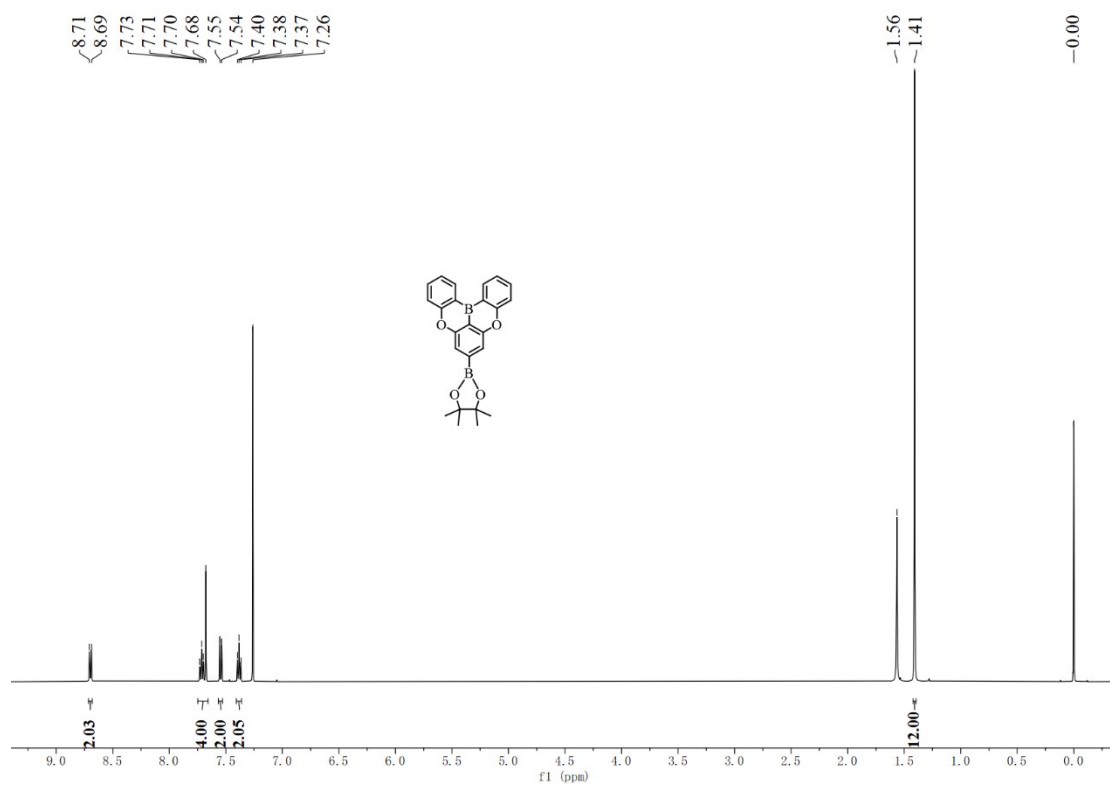


Figure S15 $^1\text{H-NMR}$ spectrum of BO-Bpin

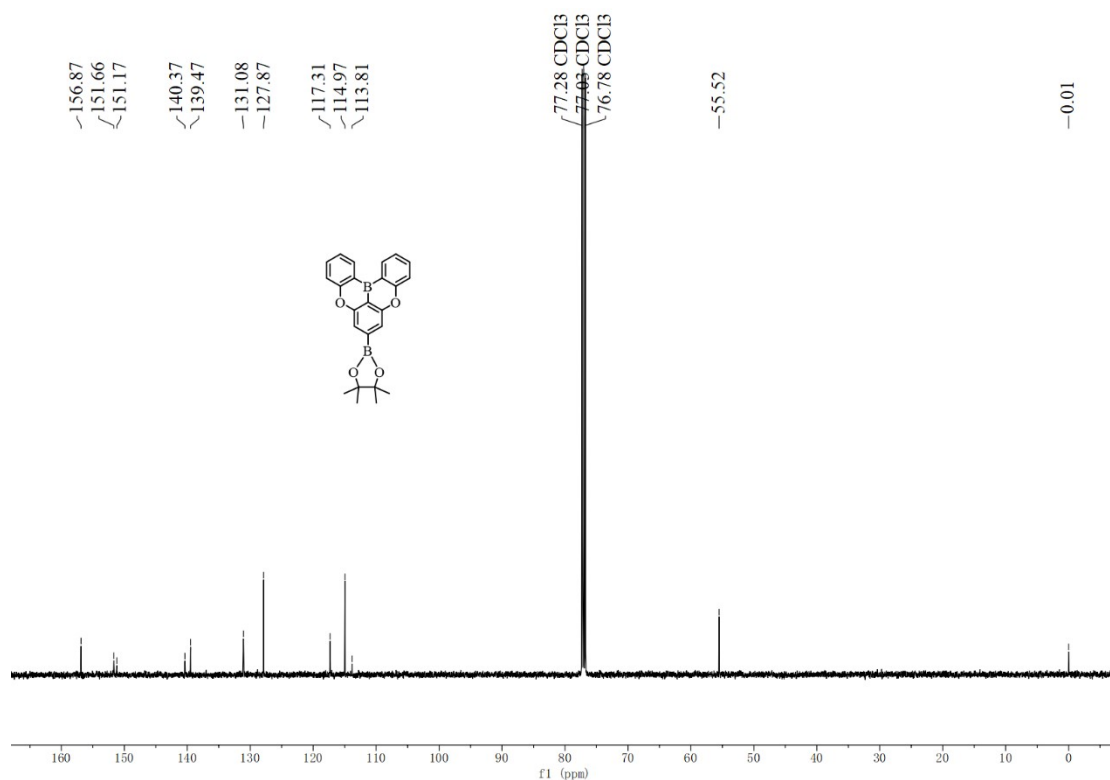


Figure S16 $^{13}\text{C-NMR}$ spectrum of BO-Bpin

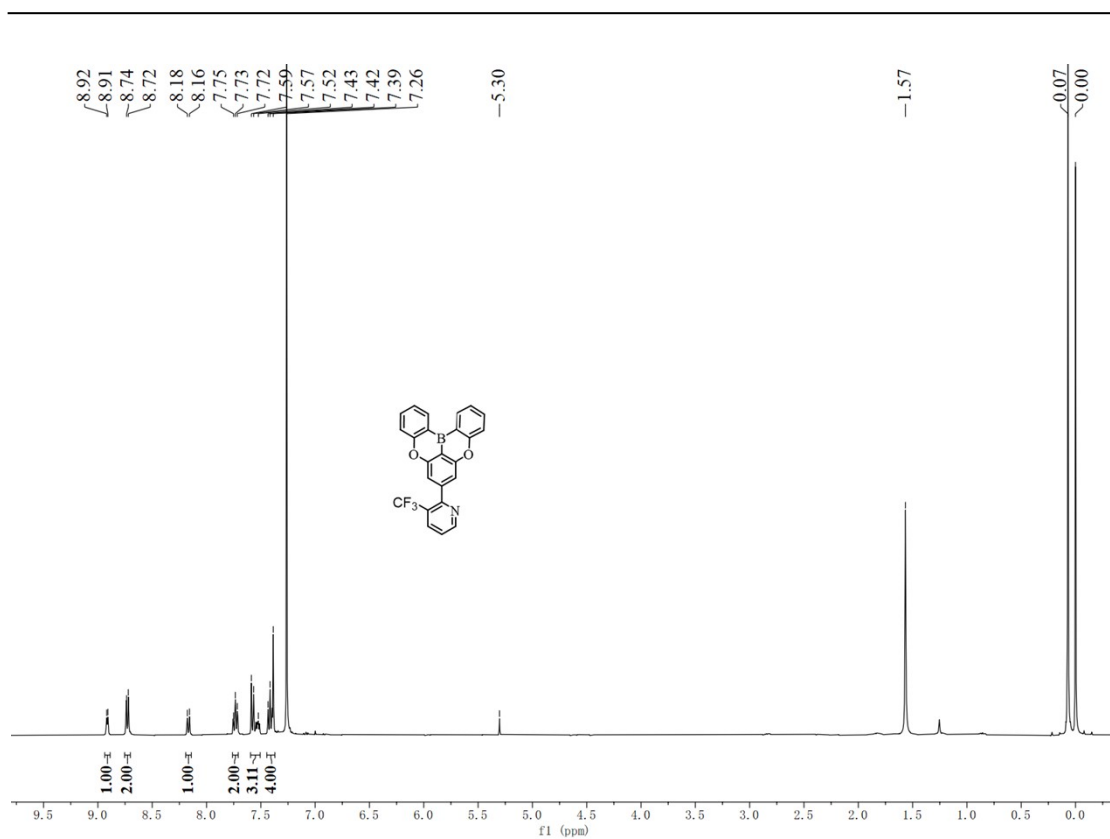


Figure S19 ^1H -NMR spectrum of free ligand BOPyH

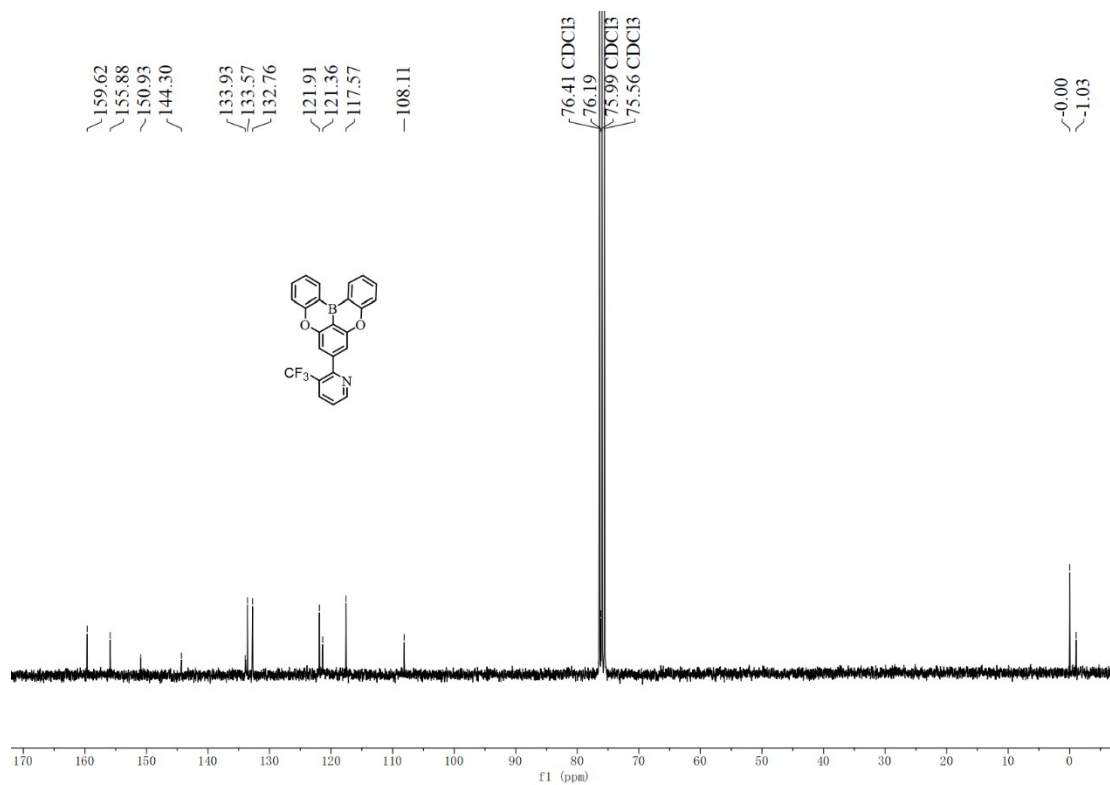


Figure S20 ^{13}C -NMR spectrum of free ligand BOPyH

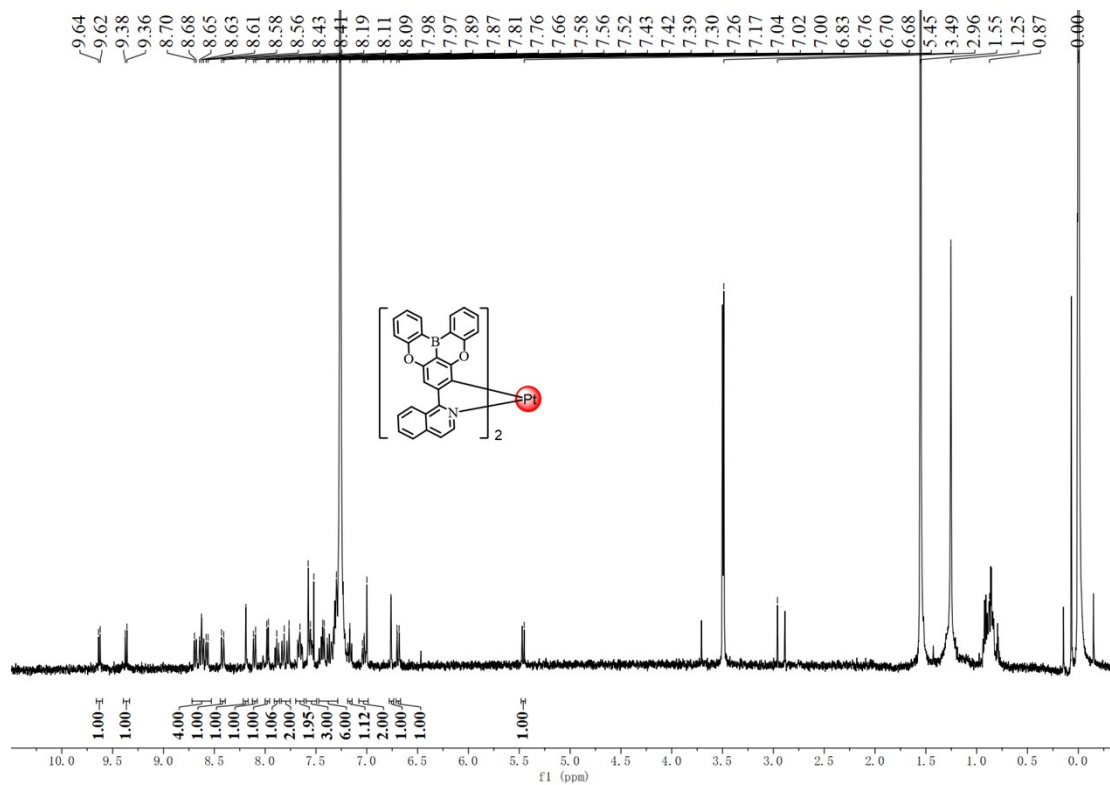


Figure S21 $^1\text{H-NMR}$ spectrum of $(\text{BOiqn})_2\text{Pt}$

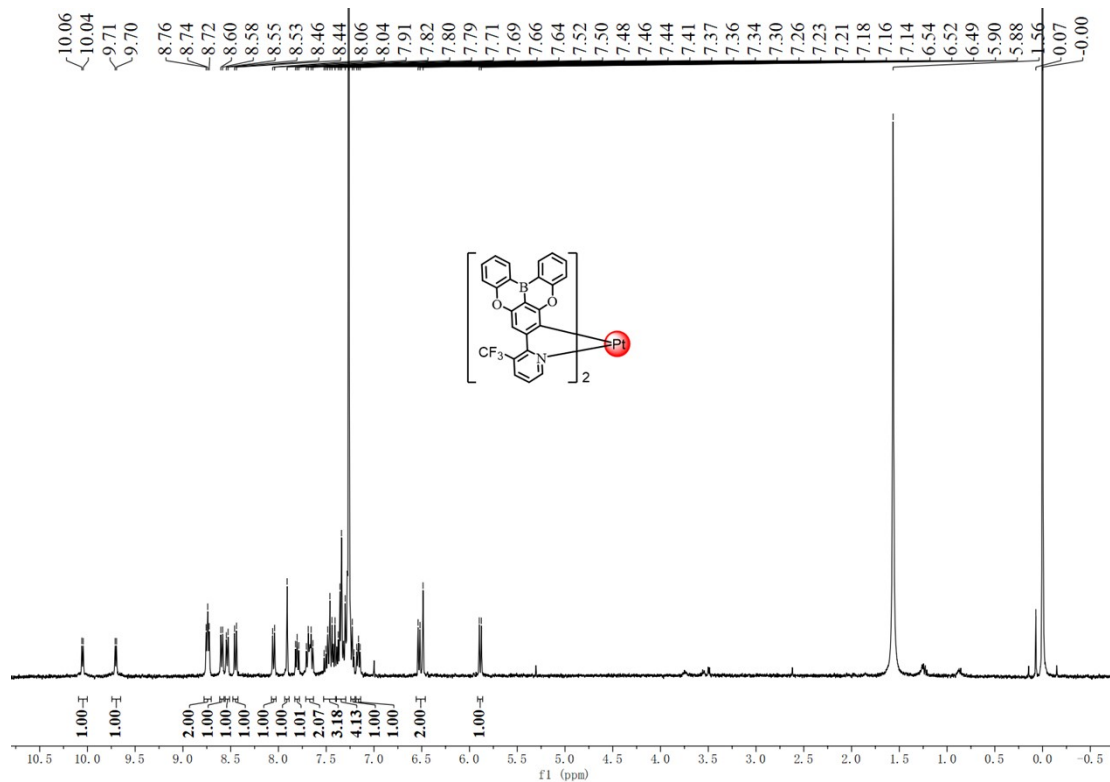


Figure S22 $^1\text{H-NMR}$ spectrum of $(\text{BOPy})_2\text{Pt}$

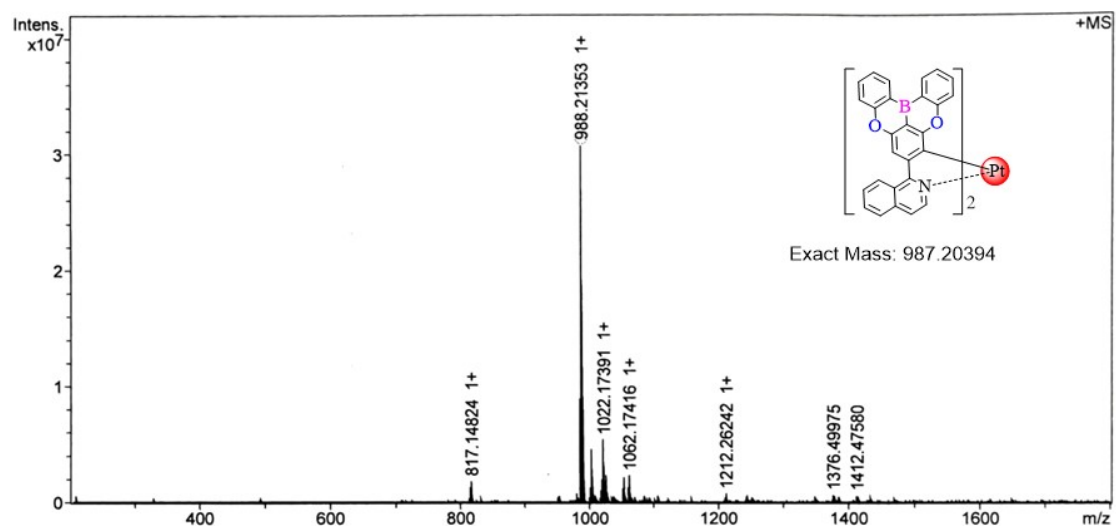


Figure S23 MALDI-TOF MS spectrum of (BOiqn)₂Pt

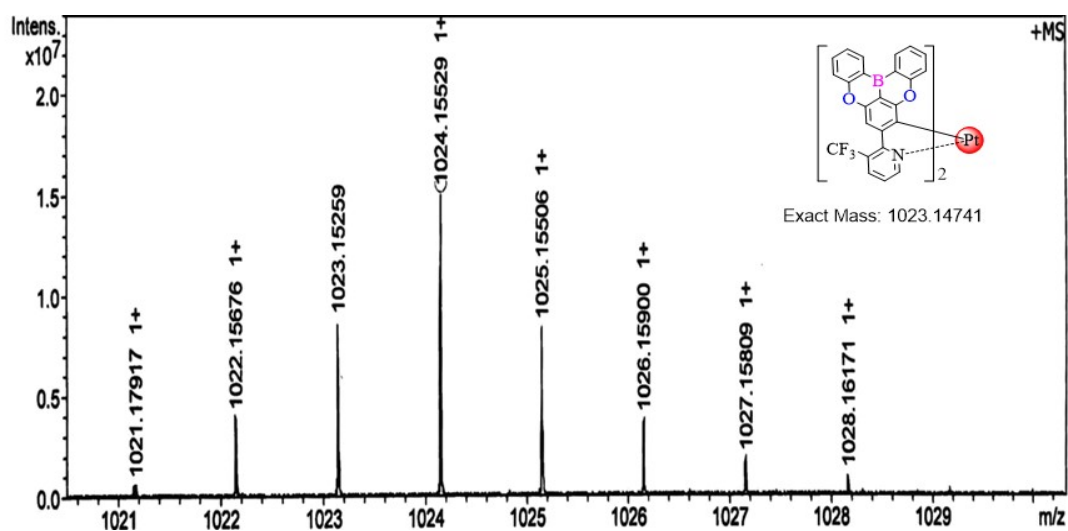


Figure S24 MALDI-TOF MS spectrum of (BOPy)₂Pt

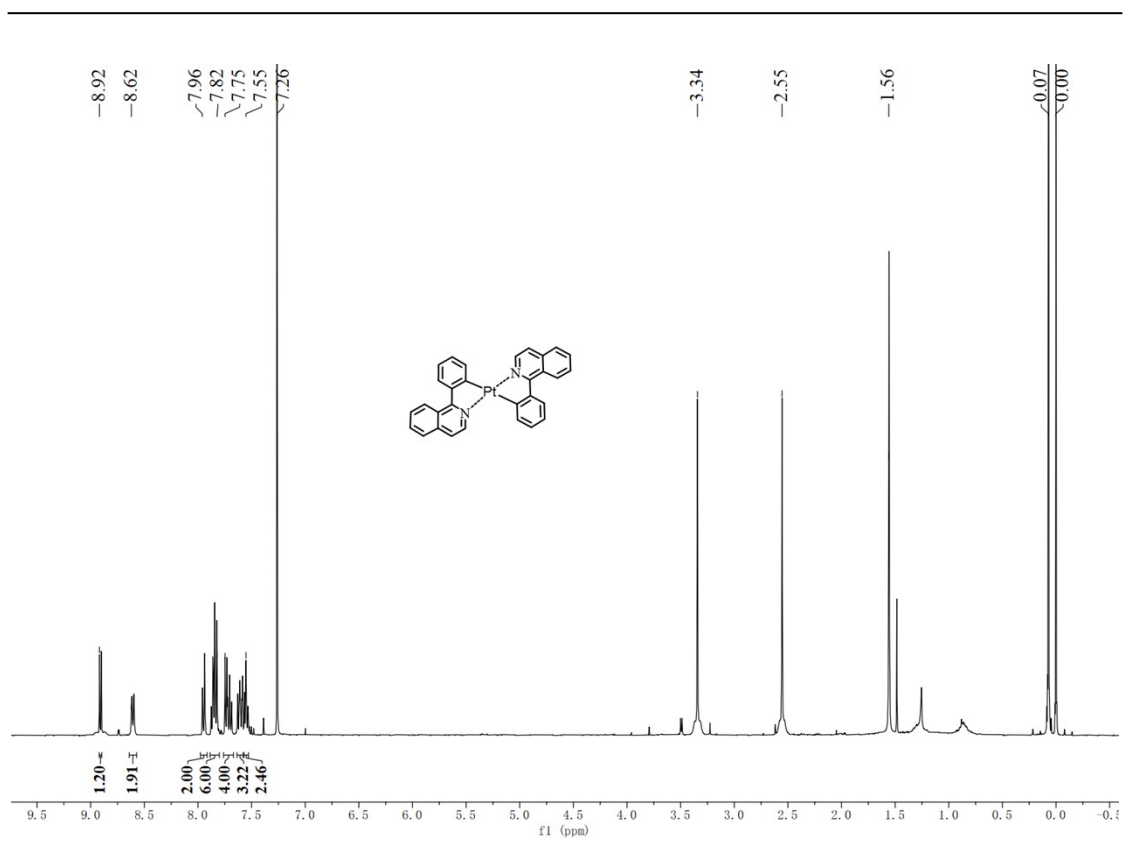


Figure S25 ^1H -NMR spectrum of $(\text{piq})_2\text{Pt}$

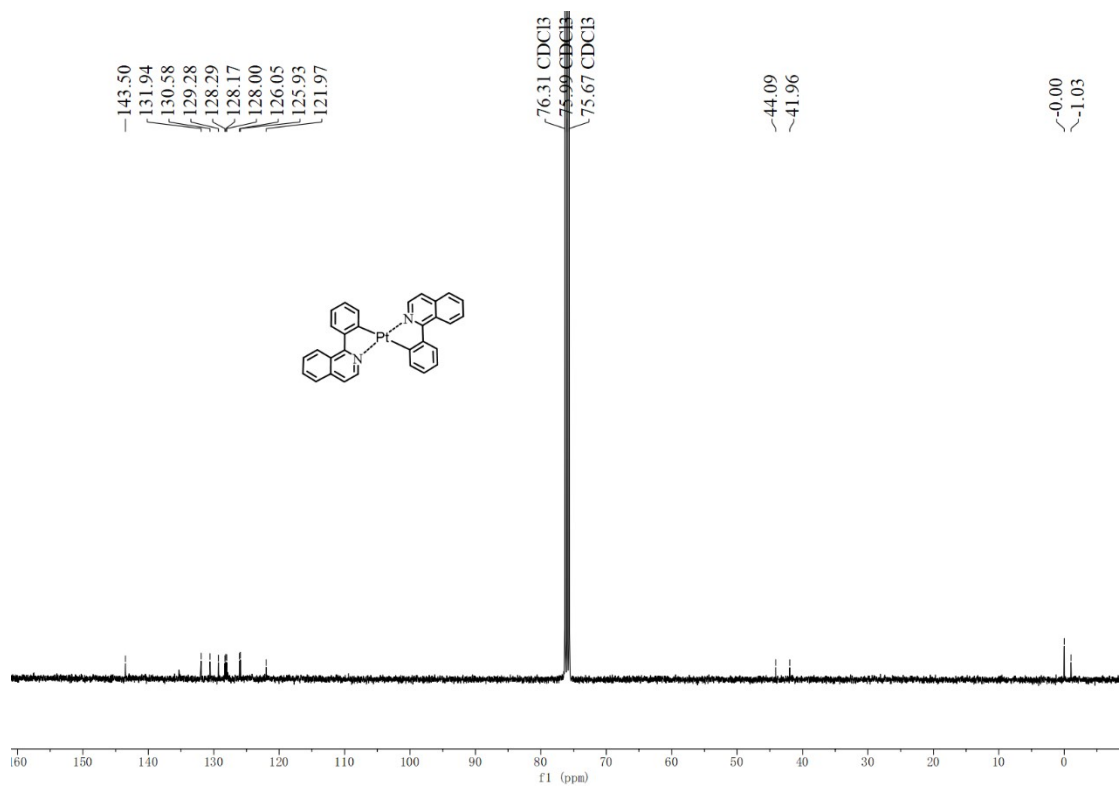


Figure S26 ^{13}C -NMR spectrum of $(\text{piq})_2\text{Pt}$